Analytical Biochemistry 413 (2011) 192–199

Contents lists available at ScienceDirect

Analytical Biochemistry

journal homepage: www.elsevier.com/locate/yabio

A genetically encoded Förster resonance energy transfer biosensor for two-photon excitation microscopy

Yuka Kumagai [a], Yuji Kamioka [b], Shunsuke Yagi [a], Michiyuki Matsuda [a,b], Etsuko Kiyokawa [b,*]

[a] Laboratory of Bioimaging and Cell Signaling, Graduate School of Biostudies, Kyoto University, Yoshida Konoe-cho, Sakyo-ku, Kyoto 606-8501, Japan
[b] Department of Pathology and Biology of Diseases, Graduate School of Medicine, Kyoto University, Yoshida Konoe-cho, Sakyo-ku, Kyoto 606-8501, Japan

ARTICLE INFO

Article history:
Received 22 January 2011
Received in revised form 14 February 2011
Accepted 16 February 2011
Available online 23 February 2011

Keywords:
Förster resonance energy transfer
Phosphoinositides
TFP
sREACh
Cyst

ABSTRACT

Pippi (phosphatidyl inositol phosphate indicator) is a biosensor based on the principle of FRET (Förster resonance energy transfer), which consists of a pair of fluorescent proteins, CFP (cyan fluorescent protein) and YFP (yellow fluorescent protein), the PH domain sandwiched between them, and K-Ras C-terminal sequence for plasma membrane localization. Due to marked cross-excitation of YFP with the conditions used to excite CFP, initial FRET images obtained by TPE (two-photon excitation) microscopy suffered from low signal-to-noise ratio, hampering the observation of lipids in three-dimensional structures. To solve this problem, YFP and CFP in the original Pippi-PI(3,4)P_2 was replaced by sREACh (super resonance energy accepting chromoprotein) and mTFP1 (monomeric teal fluorescent protein), respectively. The biosensor was also fused with an internal control protein, mKeima, where Keima/mTFP1 indicates the FRET efficiency, and indeed epidermal growth factor stimulation increased Keima/mTFP1 in HeLa cells. This biosensor successfully showed PI(3,4)P_2 accumulation to the lateral membrane in the MDCK cyst cultured in a three-dimensional environment. Furthermore, other FRET-based biosensors for PIP_3 distribution and for tyrosine kinase activity were developed based on this method, suggesting its broad application for visualizing signal transduction events with TPE microscopy.

Biosensors based on FRET (Förster resonance energy transfer)[1] and GFP (green fluorescent protein) have been increasingly used in cell biology. These genetically encoded FRET biosensors are able to monitor the concentrations of ions, sugars, and lipids, and the activity of signaling molecules such as kinases, GTPases, and proteases (reviewed in [1]).

FRET is a process by which a "donor" fluorophore in an excited state transfers its energy to a neighboring "acceptor" molecule nonradiatively [2]. The most important factor to be considered for the choice of the pair of donor and acceptor is the overlap of the donor emission and acceptor absorption spectra. In addition to this, a high quantum yield of the donor and a high molar absorption coefficient of the acceptor are required for high FRET efficiency. Furthermore, the brighter a donor and an acceptor are, the higher the signal-to-noise ratio of the acquired FRET images. By these reasons, cyan fluorescent protein (CFP) and yellow fluorescent protein (YFP), both of which are derived from Aqueora Victoria green fluorescent protein, serve as the most widely used FRET pair in the hitherto reported genetically encoded FRET biosensors. Moreover, several research groups have developed YFP mutants dedicated for FRET, such as circular permutation Venus [3], and YPet [4], which have also accelerated the widespread use of the CFP–YFP FRET pair. Recently, owing to a narrower and red-shifted absorbance peak, mTFP1 has also been used as the donor in combination of YFP as the acceptor [5].

In many studies, the FRET efficiency of the genetically encoded FRET biosensors is measured by the donor quenching and acceptor sensitization, i.e., fluorescence intensity ratio of acceptor versus donor, which is often referred to as the sensitized FRET method [2]. To gain high signal-to-noise ratio by this method, we have to consider two spectral aberrations, spectral bleed-through of the donor and cross-excitation of the acceptor. The former is the fluorescence of the donor detected through the emission filter of the acceptor. The latter is the fluorescence from the acceptor excited through the excitation filter of the donor. In the case of intramolecular FRET biosensors, these parameters could be neglected to evaluate the level of FRET [6]; however, large spectral bleed-through of the donor and cross-excitation of the acceptor will deteriorate the signal-to-noise ratio of the FRET images.

* Corresponding author. Fax: +81 75 753 4698.
E-mail address: kiyokawa@lif.kyoto-u.ac.jp (E. Kiyokawa).

[1] *Abbreviations used:* FRET, Förster resonance energy transfer; Pippi, phosphatidyl inositol phosphate indicator; CFP, cyan fluorescent protein; YFP, yellow fluorescent protein; TPE, two-photon excitation; sREACh, super resonance energy accepting chromoprotein; mTFP1, monomeric teal fluoresent protein; FLIM, fluorescence lifetime microscopy; GFP, green fluorescent protein; PI(3,4)P_2, phosphatidylinositol (3,4) bisphosphate; PIP_3, phosphatidylinositol (3,4,5) trisphosphate; PH, pleckstrin homology; EGF, epidermal growth factor; Picchu, phosphorylation indicator of CrkII chemeric unit; TPFLIM, two-photon fluorescent lifetime imaging microscopy; PtdInss, phosphoinositides.

0003-2697/$ - see front matter © 2011 Elsevier Inc. All rights reserved.
doi:10.1016/j.ab.2011.02.021

Two-photon excitation (TPE) microscopy is a powerful method for investigating three-dimensional architecture *in vivo*. Dynamic behaviors of cells expressing fluorescent proteins or labeled with chemical dyes are visible in living tissues by the TPE microscope [7,8]. It would be reasonable to apply the FRET biosensors to TPE microscopy to visualize the spatio-temporal changes in protein activities and lipid metabolism in living tissues. In fact, CFP and YFP were used as a FRET pair in earlier studies by TPE microscopy [9]. However, there is a critical problem inherent to TPE microscopy, which hampers the application of FRET biosensors. Fluorescent proteins usually have broader spectra of absorption cross section of two photons, a measure of photon capture probability, than those of single photon absorption [10]. Therefore, the level of cross-excitation of the acceptor is markedly higher in TPE microscopy than in the conventional epifluorescence microscopy, resulting in the low signal-to-noise ratio of FRET images acquired by TPE microscopy. To alleviate this problem, several research groups quantified FRET by shortening the fluorescence lifetime of the donor, which is referred to as fluorescence lifetime microscopy (FLIM) [11]. To further improve this method, a YFP variant, REACh, was developed as a nonfluorescent (“dark”) acceptor for FRET analysis [12].

Although FLIM is theoretically solid, the setting-up of a TPE microscope for this method requires expertise in physics. Considering the recent profusion of TPE microscopes among cell biologists, FRET biosensors must be improved for use with the commercially available TPE microscopes. Here, we have developed a FRET biosensor comprising TFP and REACh as the FRET pair and a fluorescent protein with large Stokes shift, Keima [13], as the internal standard of biosensor concentration. As a proof of the principle, we developed a FRET biosensor for $PI(3,4)P_2$ and observed the lipid distribution in three-dimensional structure, and extended the application to other biosensors for PIP_3 distribution and tyrosine kinase activity.

Materials and methods

Plasmids and FRET biosensors

pCX4neo-mKeima-P2A-sREACh-TAPP1 and pCX4neo-mKeima-P2A-Venus-TAPP1 for the coexpression of mKeima with sREACh-TAPP1 or Venus-TAPP1 proteins, respectively, utilized the self-cleaving 2A peptide from porcine teschovirus-1 [14]. pCAGGS-CFP-X and pCAGGS-YFP-X encode CFP (aa 1–237) and monomeric YFP (aa 1–237) with the C-terminal region of K-Ras (aa 169–188, denoted as X), respectively.

Plasmids for FRET-based monitors were constructed essentially as described previously [15,16]. The original version of the FRET biosensor for $PI(3,4)P_2$, phosphatidylinositol phosphate indicator (Pippi)-$PI(3,4)P_2$-CY, consisted of cyan fluorescent protein (aa 1–237), a spacer $(Glu–Ala–Ala–Ala–Arg)_6$, the PH domain of TAPP1 (aa 18–130), a spacer $(Glu–Ala–Ala–Ala–Arg)_3$–Gly–Gly–$(Glu–Ala–Ala–Ala–Arg)_3$, yellow fluorescent protein (aa 1–237), a spacer $(Glu–Ala–Ala–Ala–Arg)_7$, and the C-terminal region of K-Ras (aa 169–188). The YFP in the original Pippi-$PI(3,4)P_2$-CY was replaced with sREACh (aa 1–237) [17]. As an internal control, mKeima [13] was fused at the N-terminal of the biosensor, and the resultant biosensor was named Pippi-$PI(3,4)P_2$-KCS, standing for mKeima-CFP-sREACh. Similarly, the CFP in the Pippi-$PI(3,4)P_2$-KCS was replaced by enhanced green fluorescent protein (EGFP) (aa 1–237), or monomeric teal fluorescent protein (mTFP1) (aa 1–234) [18], to generate the biosensors Pippi-$PI(3,4)P_2$-KGS, and Pippi-$PI(3,4)P_2$-KTS, respectively. As a negative control, pPippi-$PI(3,4)P_2$-R221L-KTS was generated, with an Arg 221 to Leu substitution within the critical lipid-binding motif of the PH domain. The pPippi-$PI(3,4)P_2$-KTS and pPippi-$PI(3,4)P_2$-R221L-KTS expression cassettes were transferred to Moloney murine leukemia virus (MuLV)-based retroviral vector plasmids [19], to generate pCX4neo-Pippi-$PI(3,4)P_2$-KTS and pCX4neo-Pippi-$PI(3,4)P_2$-R221L-KTS, respectively. Similarly, wild-type and mutant biosensors, pCX4neo-Pippi-PIP_3- and -PIP_3-R284C-KTS, were generated. The Arg 284 to Cys substitution lies within the critical lipid-binding motif of the PH domain.

The biosensor Picchu-KTS-X was generated from the original Picchu (phosphorylation indicator of CrkII chemeric unit)-X [20] by replacing YFP with sREACh (aa 1–237), and adding mKeima [13] at the N-terminal of the biosensor. The corresponding negative control, Picchu-Y221F-KTS-X, harbored a Tyr 221 to Phe substitution in CrkII.

Cell culture and transfection

HeLa cells were maintained in DMEM (Sigma–Aldrich, St. Louis, MO) supplemented with 10% fetal bovine serum (FBS). MDCK (Madin-Darby Canine Kidney) cells were purchased from the RIKEN BioResource Center (No. RCB0995) (Tsukuba, Japan) and maintained in MEM Earle’s salts (Invitrogen, Carlsbad, CA) supplemented with 10% FBS, 2 mM L-glutamine, and 1 mM sodium pyruvate. For transient expression studies, HeLa cells were transfected using 293Fectin (Invitrogen), and 48 h after transfection, cells were analyzed with microscopy.

Retroviral gene transfer

To establish the MDCK cells stably expressing FRET biosensors, retroviral particles were produced in BOSC23 cells by transfection of pPippi-$PI(3,4)P_2$-KTS or -R221L-KTS, together with the plasmids pGP (the packaging plasmid) and pVSV-G (the envelope), and viral supernatant were used to infect MDCK cells. After selection with 0.5 mg/ml of G418, the cells expressing the biosensors were sorted by FACS Aria (BD Bioscience, San Jose, CA).

Spectrometry measurement

HeLa cells expressing FRET biosensors were observed with a FV-1000 confocal microscope equipped with SA100S (Olympus) for the fluorescence spectrum analysis. An LD405 laser was used for the excitation, and the emission profiles were acquired every 5 nm from 440 to 650 nm in a lambda scan mode.

FRET imaging with epifluorescence microscope

FRET imaging with epifluorescence microscopy was performed essentially as described [21]. HeLa cells were plated on 35-mm glass-base dishes (Asahi Techno Glass, Tokyo, Japan), which were coated with collagen type I (Nitta Gelatin Inc., Osaka, Japan), and maintained in phenol red-free DMEM F12 (Invitrogen). Cells transfected with plasmids were imaged every 1 min for 30 min with the inverted microscope (IX71; Olympus, Tokyo, Japan) equipped with a Cool SNAP-HQ-cooled charge-coupled device camera (Roper Scientific, Trenton, NJ) controlled with MetaMorph software (Universal Imaging, West Chester, PA). In some experiments, cells were stimulated with 50 ng/ml epidermal growth factor (EGF) during the imaging. Cells were illuminated with a 75-W xenon lamp through a 12% ND filter (Olympus) and a 60x oil immersion objective lens (PlanApo 60x/NA 1.4).

The spectral characterization of fluorescent protein used in this study is summarized in Table S1. The filter settings for individual experiments are summarized in Supplemental Fig. S1 and Table S2, and as follows.

Direct excitation assay (Fig. 1): excitation filter, XF1071/440AF21 for CFP or S492/18x for YFP; dichroic mirror, 86006bs; emission filters, XF3075/480AF30 for CFP and XF1019/535AF26 for YFP. All filters were obtained from Omega Optical (Brattleboro, VT).

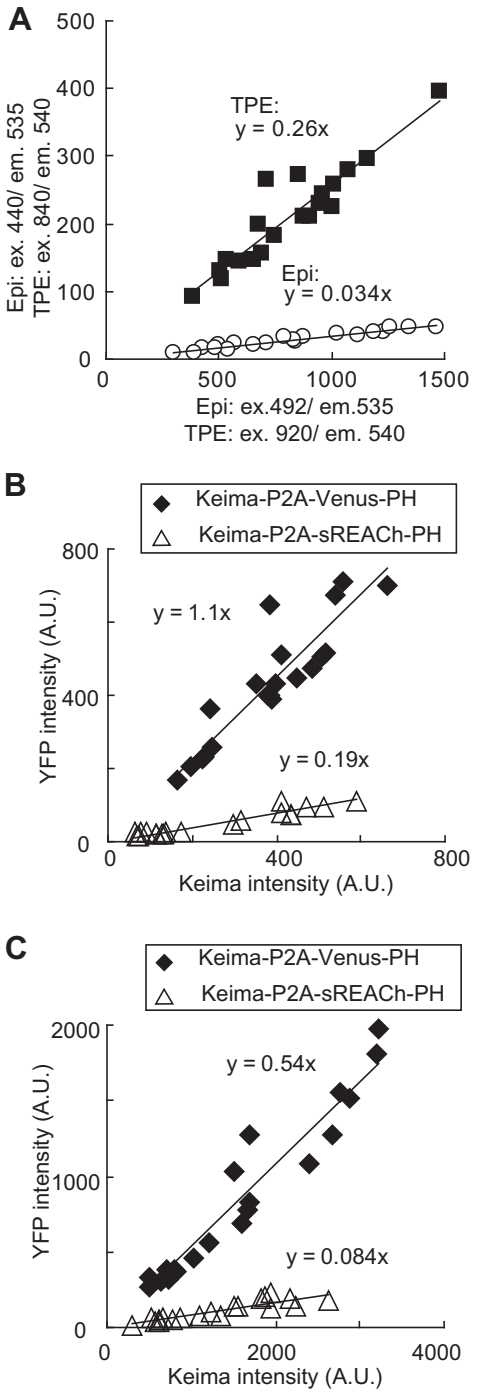

Fig.1. Fluorescence properties of YFP and sREACh under epifluorescent and two-photon microscopes. (A) HeLa cells expressing Venus were excited through a bandpath filter of 440AF21 or S492/18 and imaged through a bandpath filter 535AF26 with an epifluorescence microscope (open circle), or excited at 840 or 920 nm and imaged through a bandpath filter BP520–560 with a two-photon microscope (filled squares). The net fluorescence intensity averaged over each cell was plotted and approximated to a liner line. $n = 20$. (B) HeLa cells expressing mKeima-P2A-Venus-TAPP1 (filled diamond) or mKeima-P2A-sREACh-TAPP1 (open triangle) were excited through a bandpath filter of S492/18 and imaged through a bandpath filter 535AF26 or 635DF55 with an epifluorescence microscope. $n = 20$. (C) HeLa cells expressing mKeima-P2A-Venus-TAPP1 (closed diamond) or mKeima-P2A-sREACh-TAPP1 (open triangle) were excited at 840 nm and imaged through a bandpath filter BP520-560 or a dichroic mirror SDM 570 with a two-photon microscope. $n = 20$.

Time lapse imaging for Pippi-PI (3,4)P_2-KCS and -KTS (Fig. 3): excitation filter, an XF1071/440AF21 (Omega) or S492/18x (Chroma (Bellows Falls, VT)); dichroic mirror, 86006bs (Omega); emission filters, XF3075/480AF30 (Omega) for donor proteins (CFP and TFP), and XF3015/635DF55 (Omega) for Keima.

Time lapse imaging for Pippi-PI (3,4)P_2-KGS (Fig. 3): Excitation filter, an XF1071/440AF21 (Omega) or S492/18x (Chroma); dichroic mirror, 86006bs (Omega); emission filters, XF3040/510WB40 (Omega) for GFP, and XF3015/635DF55 (Omega) for Keima.

FRET imaging with a two-photon microscope

HeLa cells expressing FRET biosensors were prepared as described above. Images were obtained with a two-photon microscope (BX61WI; Olympus), which was controlled with Fluoview (Olympus). For time-lapse imaging, cells were imaged every 2 min for 30 min. At each time point, images were acquired in four z-slices (depth 12 μm), stacked into one image, and background was subtracted. In some experiments, cells were stimulated with 50 ng/ml of EGF. Cells were illuminated with an 840 nm (1.5%) Ti-Sapphire laser (Mai-Tai DeepSee HP (Spectra-Physics, Tokyo)) tuned to an 840 nm excitation with 100 fs pulses at 80 MHz, and visualized with a 25× immersion objective lens (XLPLN25XWMP, Olympus,). Detailed imaging settings are summarized in Supplemental Fig. S1 and Table S2, and as follows.

Direct excitation assay (Fig. 1): laser power for excitation, 840 nm (1.5%) and 920 nm (1.5%); dichroic mirror, SDM 570 (Olympus); emission filters, BP460-500 for CFP and BP520-560 for YFP variants. For Keima, the light from 570 nm was acquired. Scan speed, 100 μs/pix; pixel size, 521 × 521.

Time lapse imaging (Figs. 3, 5 and 6): laser power for excitation, 840 nm (1.5%); dichroic mirror SDM 570 (Olympus), emission filters for donors, BP460-500 for CFP and TFP, BP520-560 for YFP and GFP; for Keima, the light from 570 nm was acquired without an emission filter. Scan speed, 12.5 μs/pix; pixel size, 320 × 320.

MDCK cystogenesis

Cysts and tubules were generated as previously described [22,23]. Briefly, 7.5×10^3 MDCK cells were placed on a glass coverslip (13 mm in diameter) coated with 90 μl of polymerized Matrigel (BD Biosciences, Bedford, MA). Cells were cultured in 2% Matrigel/culture medium for indicated periods (see Results).

Acquisition of 3D images with a two-photon microscope

The Pippi-PI(3,4)P_2-KTS expressing MDCK cysts were imaged with a two-photon microscope operated by Fluoview. The image data were transferred to Metamorph. After background subtraction, the Keima/TFP ratio images were transferred to Imaris (Bitplane AG) to reconstitute a 3D image. At the same time, the fluorescent intensities corresponding to the apical and lateral membranes were obtained with the linescan function in Metamorph, and transferred to Excel (Microsoft). Detailed imaging settings are as follows.

Slice images (Fig. 4): laser power, 840 nm (1.0–2.0%); the filters used for this experiment were the same as for time lapse imaging with two-photon microscopy; pixel size, 512 × 512; scan speed, 100 μs/pix.

Processing the graphs and statistics

After subtracting the background in Metamorph Software, information for the averaged intensity and cell area was exported to the Excel software (Microsoft). For statistics in Fig. 4, FRET efficiencies were analyzed by a two-tailed paired Student's *t* test.

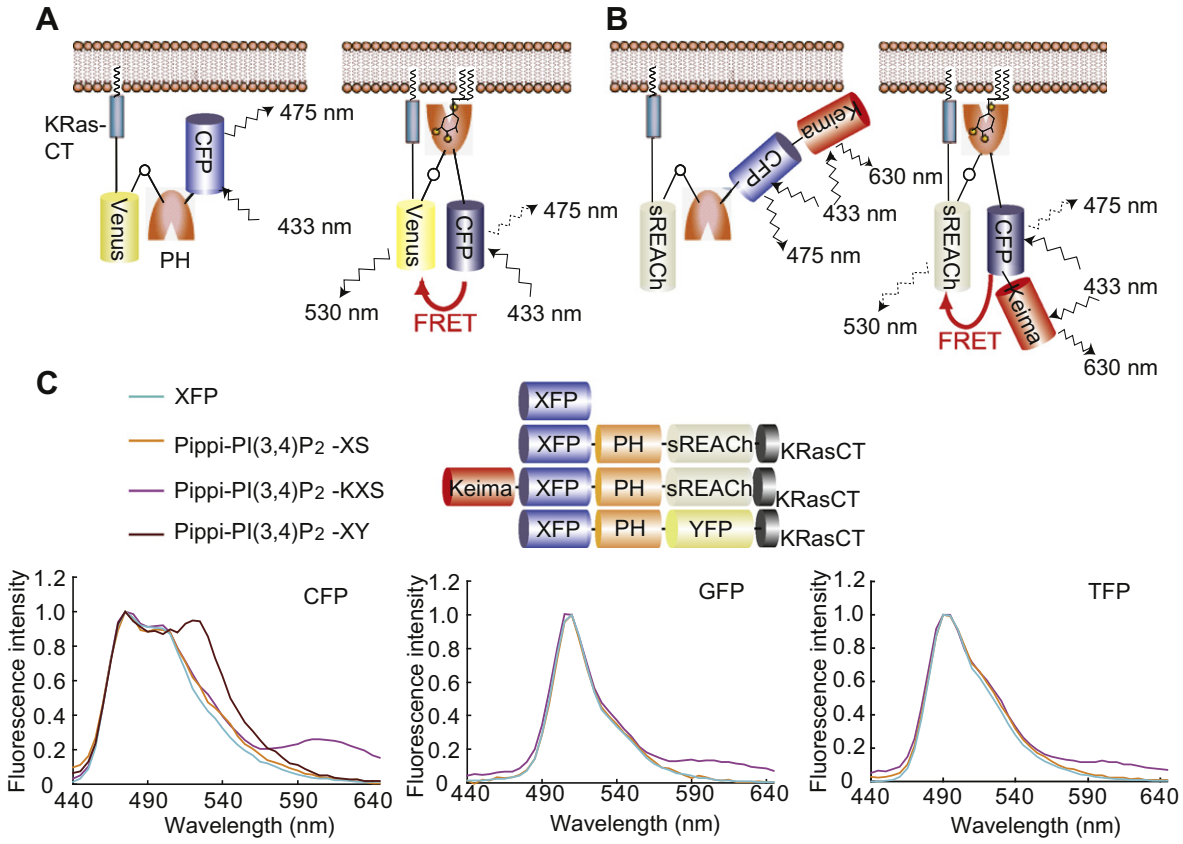

Fig.2. Development of FRET bisosensor for PI(3,4)P_2 with sREACh. (A) Schematic representation of the original version of Pippi-PI(3,4)P_2. YFP and CFP denote a yellow-emitting mutant of GFP and cyan-emitting mutant of GFP, respectively. K-Ras4B-CT indicates the C-terminal region of K-Ras4B, and Gly–Gly indicates a glycine–glycine linker. The PH domain of TAPP1 was utilized as the PI(3,4)P_2-binding domain. In this biosensor design, the FRET level will increase when the biosensor recognizes PI(3,4)P_2. (B) Schematic representation of the improved version of Pippi-PI(3,4)P_2. sREACh and CFP denote a yellow-emitting mutant of GFP and cyan-emitting mutant of GFP, respectively. K-Ras4B-CT indicates the C-terminal region of K-Ras4B, and Gly–Gly indicates a glycine–glycine linker. The PH domain of TAPP1 was utilized as the PI(3,4)P_2-binding domain. Keima was fused at the N terminal as an internal control. In this biosensor design, the FRET level is indicated by the Keima/CFP ratio and will increase when the biosensor recognizes PI(3,4)P_2. (C) The HeLa cells expressing FRET biosensors indicated above were observed with a FV-1000 confocal microscope for the fluorescence spectrum analysis. A single cell was illuminated with an LD405 laser for the excitation, and emission profiles from 440 to 650 nm in a lambda scan mode were acquired. After background subtraction, the results were normalized at its maximum emission intensity. The graph represents the average from 10 cells.

Results

Properties of YFP variants in epifluorescent and two-photon microscopes

To improve current FRET biosensors using CFP and YFP for application in two-photon excitation microscopy, we designed a biosensor using sREACh as an acceptor and mKeima as an internal standard of the biosensor concentration. REACh is a YFP variant with extremely low quantum efficiency and high absorbance [12]. This property renders sREACh an appropriate acceptor in FRET imaging by two-photon fluorescent lifetime imaging microscopy (TPFLIM) [17]. In TPFLIM, FRET is measured by the shortening of CFP lifetime. Although this method is theoretically rigid, most commercially available TPE microscopes are not equipped with the detector of fluorescence lifetime. Thus, in our biosensor design, the level of FRET was measured by the decrease in CFP fluorescence intensity using another fluorescent protein, mKeima, as an internal standard of biosensor concentration. Taking advantage of the long Stokes' shift, mKeima can be excited at an excitation wavelength used for CFP without perturbing the detection of FRET [13]. Before constructing new FRET biosensors, we examined the properties of YFP variants in epifluorescence and TPE microscopes.

First, the level of cross-excitation of Venus, a bright YFP variant [24], was compared between epifluorescence and TPE microscopes. HeLa cells expressing Venus were imaged under conditions used to acquire FRET images (ex. 440 or 840 nm, and em. 530 nm) or those used to acquire YFP images (ex. 480 or 920 nm, and em. 530 nm). Acquired FRET images reflect the level of cross-excitation. Fluorescence intensities averaged over each cell area are plotted in Fig. 1A. The slopes of the fitted lines showed that the cross-excitation was about eight times larger in a TPE microscope than in an epifluorescent microscope. Thus, we concluded that reduction of cross-excitation of YFP would significantly improve the signal-to-noise ratio of FRET images when TPE microscopes are applied.

Next, the level of cross-excitation was compared between sREACh and Venus in both epifluorescence and TPE microscopes. For this purpose, we constructed plasmids for the expression of mKeima-P2A-sREACh and Venus-P2A-sREACh, in which the self-cleaving 2A peptide was used to ensure equimolar expression of mKeima and YFP variants [14]. As in Fig. 1A, the level of cross-excitation was quantified except that fluorescence intensity of mKeima was used as an internal standard. As reported previously [12], the fluorescence intensity of sREACh was markedly lower than that of Venus, in both epifluorescence (Fig. 1B) and TPE microscopes (Fig. 1C), respectively. These results indicate that sREACh could significantly reduce the level of cross-excitation of the acceptor protein and thereby improve the signal-to-noise ratio in FRET imaging with a TPE microscope.

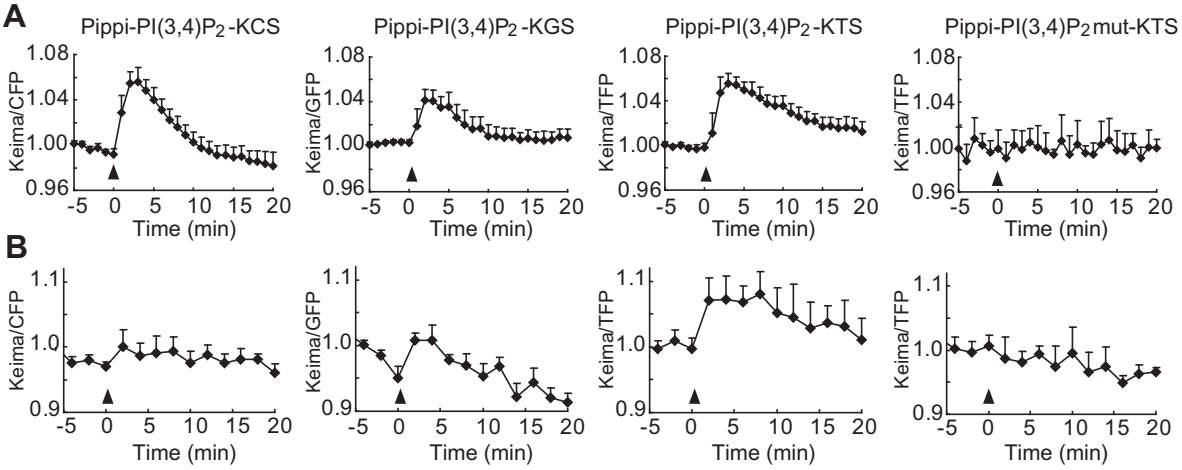

Fig.3. Time-lapse FRET imaging. (A) HeLa cells were transfected with plasmids for the biosensors indicated above. Two days later, the cells were starved for 5 h, and stimulated with 50 ng/ml of EGF. Donor (ex. 440 ± 21 nm, em. 480 ± 30 nm) and Keima (ex. 440 ± 21 nm, em. 635 ± 55 nm) images were obtained every 1 min for 30 min with a time-lapse epifluorescent microscope. The net intensities of Keima and donor fluorescent proteins in each cell were measured to calculate the averaged emission ratio (Keima/donor). The Keima/donor ratio was normalized by the average value before stimulation. The graph shows the average + the standard deviation (SD). The number of cells examined in each case was as follows: 11 (Pippi-PI(3,4)P2-KCS), 10 (Pippi-PI(3,4)P2-KGS), 13 (Pippi-PI(3,4)P2-KTS), and 9 (Pippi-PI(3,4)P2-R221L-KTS). (B) HeLa cells were transfected with plasmids for the biosensors indicated above. Two days later, cells were starved for 5 h, and stimulated with 50 ng/ml of EGF under two-photon microscopy as described under Materials and methods. Images were obtained every four z-slices (interval 3 μm), every 2 min for 30 min. Images at the same time point were then stacked into one image. The net intensities of donor and Keima in each cell were measured to calculate the Keima/donor ratio. The graph shows the average + the standard deviation (SD). The number of cells examined in each case was as follows: 5 (Pippi-PI(3,4)P2-KCS), 5 (Pippi-PI(3,4)P2-KGS), 7 (Pippi-PI(3,4)P2-KTS), and 4 (Pippi-PI(3,4)P2-R221L-KTS).

FRET biosensors with sREACh and mKeima

Among various FRET biosensors, Pippi-PI(3,4)P_2 was selected in the pilot study for the biosensor improvement, since localized accumulation of PI(3,4)P_2 is important for polarity formation in the two-dimensional environment, such as cell migration and axon guidance [25,26]; therefore, it is worth visualizing its distribution in a three-dimensional system. The PH domain of Pippi-PI(3,4)P_2 binds to PI(3,4)P_2 on the plasma membrane and brings CFP in close proximity to YFP, thereby increasing FRET efficiency from CFP to YFP (Fig. 2A) [16,27]. In the prototype Pippi-PI(3,4)P_2 (which we call Pippi-PI(3,4)P_2-CY in this study) FRET was quantified by the fluorescence intensity ratio of Venus versus CFP. In the new FRET biosensor, Pippi-PI(3,4)P_2-KCS (KCS stands for Keima-CFP-sREACh), YFP was replaced by sREACh and mKeima was fused to the N-terminus (Fig. 2B). In this biosensor design, FRET is manifested by the decrease of CFP fluorescence, which can be quantified as the fluorescence ratio of Keima versus CFP.

Comparison of the fluorescence spectrum of Pippi-PI(3,4)P_2-CY with that of Pippi-PI(3,4)P_2-CS, in which CFP in Pippi-PI(3,4)P_2-CY was replaced with sREACh, showed that fluorescence from sREACh was almost negligible (Fig. 2C). Comparison of the fluorescence spectrum of Pippi-PI(3,4)P_2-CS with that of Pippi-PI(3,4)P_2-KCS showed that the fluorescence from mKeima could be easily separated from that of CFP.

We could replace CFP with other fluorescence proteins having a longer fluorescent wavelength in the sREACh-based FRET biosensors, because spectral overlap between the donor and acceptor fluorescence proteins would not perturb the detection of FRET. In addition, the fluorescence of CFP was known to be relatively low in comparison with other fluorescent proteins such as TFP and GFP [28,29]. Thus, to further improve the FRET biosensors for Pippi-PI(3,4)P_2, CFP was replaced with GFP and TFP, generating Pippi-PI(3,4)P_2-KGS and -KTS, respectively. The relative fluorescence intensities of mKeima to GFP and TFP in these biosensors were lower than that of mKeima to CFP in Pippi-PI(3,4)P_2-KCS; moreover, the spectral separation between the donor and mKeima was found to be sufficient (Fig. 2C).

Comparison of the sensitivity of biosensors with various FRET donors in EGF-stimulated cells

To compare the sensitivity of the biosensors with different FRET donors, HeLa cells expressing Pippi-PI(3,4)P_2-KCS, -KGS, and -KTS were stimulated with EGF and analyzed with a conventional epifluorescent microscope and a TPE microscope (Fig. 3). HeLa cells expressing a mutant biosensor, Pippi-PI(3,4)P_2-mut-KTS, were also used as a negative control. In this construct, Pippi-PI(3,4)P_2-R221L-KTS, Arg221, which is critical for the recognition of PI(3,4)P_2, was replaced by Leu. The production of PI(3,4)P_2 and the resulting increase in FRET were monitored by the fluorescence intensity of mKeima versus that of the donor fluorophore excited at 440 nm. With an epifluorescence microscope (Fig. 3A), all biosensors except Pippi-PI(3,4)P_2mut-KTS responded on EGF stimulation to a similar extent, 4–5% on average. However, with a TPE microscope (Fig. 3B), Pippi-PI(3,4)P_2-KTS responded significantly higher than on Pippi-PI(3,4)P_2-KCS and -KGS on EGF stimulation. These results indicate that TFP serves as the best donor for sREACh at least in the structure of Pippi-PI(3,4)P_2.

PI(3,4)P_2 distribution in the three-dimensional structures

The major advantage of the TPE microscopy is its capability to observe the thick samples. Since phosphoinositides (PtdInss) have been reported to play important roles in maintenance of the three-dimensional architectures [22], we decided to examine the PI(3,4)P_2 distribution in the MDCK cysts. MDCK cells form monolayer spheroid structures, called cysts, when cells grow in the Matrigel [30]. To investigate the PI(3,4)P_2 distribution, MDCK cells expressing Pippi-PI(3,4)P_2-KTS or -R221L-KTS were established by retroviral infection, cultured in the Matrigel, and observed with a TPE microscope. As shown in Fig. 4A, FRET efficiency of the wild-type biosensor, but not the mutant one, was higher at the lateral membrane than at the apical membrane. Quantitative analysis from various cysts revealed that the PI(3,4)P_2 was accumulated significantly to the lateral membrane (Fig. 4B). Such uneven distribution was not observed in the cysts expressing the mutant biosensor

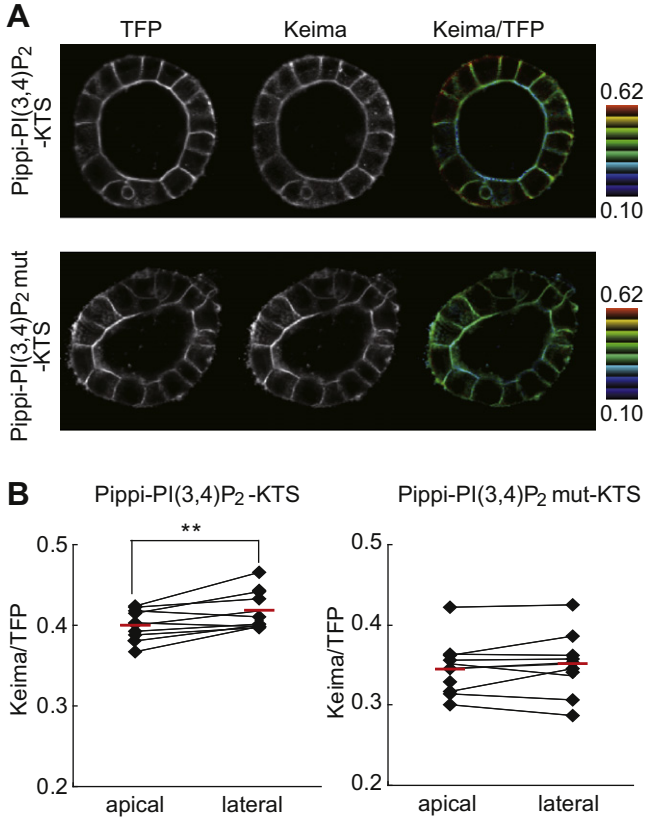

Fig.4. PI(3,4)P_2 distribution in the MDCK cyst. (A) Representative FRET images of MDCK cysts expressing Pippi-PI(3,4)P_2-KTS and Pippi-PI(3,4)P_2mut-KTS were obtained by TPE microscopy. The calculated FRET efficiency is differentiated by color in intensity-modulated display (IMD) modes shown at the right. The upper and lower limits of the ratio range are also shown at the right. The scale bar indicates 10 μm. (B) After subtracting background, the fluorescence of corresponding to the apical and lateral membranes from Keima and TFP images was measured with the "linescan" function (MetaMorph), transferred to Excel (Microsoft) to calculate the Keima/TFP ratio at apical and lateral membranes, and examined for statistical significance by paired analysis from the same cyst. The red bars in the graph indicate the average. The asterisk indicates the significance of the paired Student's *t* test ($^{**}P < 0.01$).

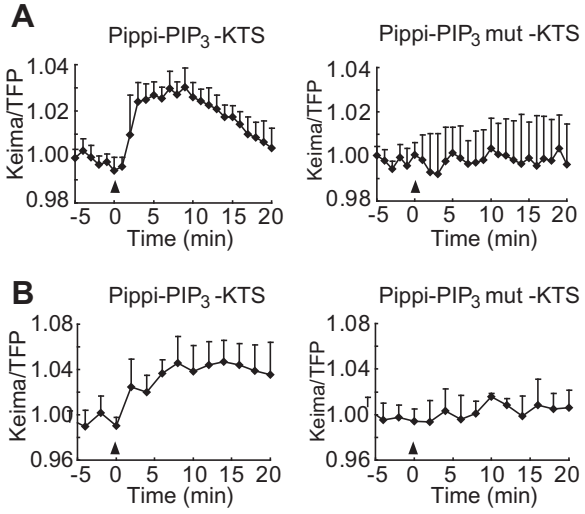

Fig.5. Generation of Pippi-PIP_3-KTS. (A) HeLa cells expressing the biosensors indicated above were stimulated with EGF and processed as in Fig. 3A. The number of cells examined in each case was as follows: 10 (Pippi-PIP_3-KTS), 10 (Pippi-PIP_3mut-KTS). (B) HeLa cells expressing the biosensors indicated above were stimulated with EGF and processed as in Fig. 3B. The number of cells examined in each case was as follows: 6 (Pippi-PIP_3-KTS) and 6 (Pippi-PIP_3mut-KTS).

(Fig. 4B, the right graph). Of note, the overall Keima/TFP of the mutant biosensor was lower than that of the wild-type, indicating that this biosensor detected the basal level of PI(3,4)P_2 in the cysts.

Generation of the FRET biosensors for PIP_3 and tyrosine kinase activity with sREACh and mKeima

The above results indicate that the biosensor backbone with mKeima, mTFP, and sREACh detects PI(3,4)P_2 under the TPE microscope. We next sought to apply this strategy to other Pippi biosensors. For this, the PH domain of Pippi-PI(3,4)P_2-KTS was replaced by that from GRP, which binds specifically to PIP_3. The resultant FRET biosensor Pippi-PIP_3-KTS was expressed in HeLa cells and examined as in Fig. 3. In both epifluorescent and TPE microscopes, Pippi-PIP_3-KTS showed an increase in FRET ratio on EGF stimulation (Fig. 5A and B, left). In contrast, the biosensor with an Arg to Cys mutation at residue 284 in the PH domain (Pippi-PIP_3mut-KTS) showed no significant change in FRET ratio, indicating that Pippi-PIP_3-KTS specifically detected PIP_3 on EGF stimulation.

Lastly, using the same strategy, Picchu-KTS-X, a FRET biosensor for tyrosine kinase activity, was generated. The proto-type of Picchu-X consisted of YFP, CrkII, CFP, and the C-terminal region of K-Ras [20]. On EGF stimulation, the Tyr 221 of CrkII is phosphorylated, which is recognized by its SH2 domain. This intramolecular binding brings CFP close to YFP and increases the FRET from CFP to YFP (Fig. 6A). As shown in Fig. 6B and C, Picchu-KTS-X increased in FRET ratio up to 8% and 10% under the epifluorescent and TPE microscopes, respectively. The biosensor with Tyr 221 mutated to Phe (Picchu-mut-KTS-X) did not respond to EGF in either microscope, indicating that FRET of Picchu-KTS-X was increased on its tyrosine phosphorylation, and thereby demonstrating the utility of Picchu-KTS-X for the monitoring of kinase activity in living cells by TPE microscopy.

Discussion

Our objective is a genetically encoded FRET biosensor that can be used in commercially available TPE microscopes without additional instruments. Considering the prevalence of CFP and YFP as the donor and acceptor fluorescence proteins, respectively, among the hitherto developed genetically encoded FRET biosensors, we used a PI(3,4)P_2 biosensor, Pippi-PI(3,4)P_2 comprising CFP and YFP, as the prototype for improvement. The rationale for our modifications to the biosensors involves considerations of both the acceptor and the donor.

Acceptor preference: The critical difference between epifluorescence and TPE microscopes is the method to excite the donor. In an epifluorescence microscope, a narrow bandpass excitation filter can minimize the cross-excitation of the acceptor; whereas in a TPE microscope the spectrum of absorption cross section of two photons is assumed to be broad, causing a significant level of cross-excitation (Fig. 1). In most TPE microscopes without the instruments for measuring fluorescence lifetime, FRET is detected by the ratiometry of donor intensity versus acceptor intensity (sensitized FRET); therefore, large cross-excitation of the acceptor reduces the signal-to-noise ratio of the acquired FRET images. Indeed in our system, Venus was cross-excited at 840 nm by a TPE microscope (Fig. 1), although the two-photon absorption peak of YFP is reported to be near

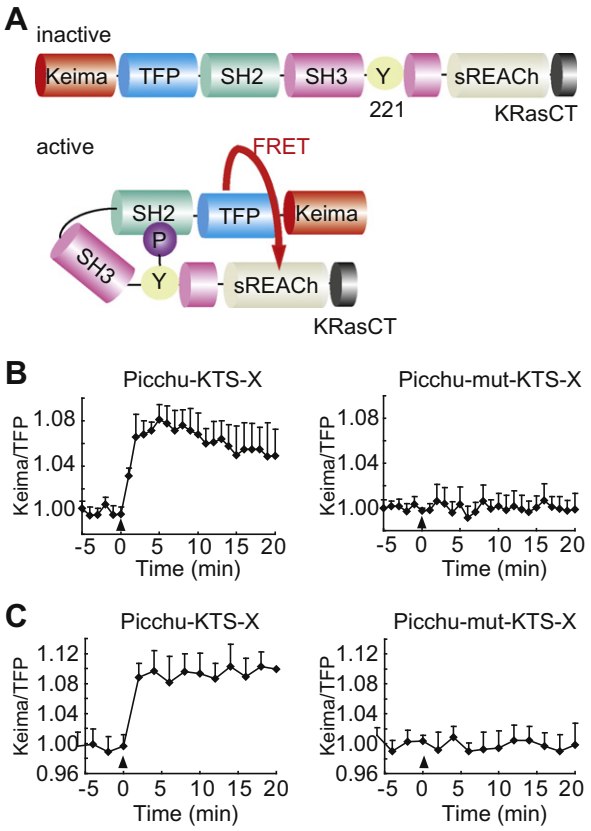

Fig.6. Generation of Picchu-KTS-X. (A) Schematic representation of Picchu-KTS-X. The SH2 domain of CrkII was utilized as the phosphorylated tyrosine at residue 221. In this biosensor design, the FRET level is indicated by the Keima/TFP ratio and will increase when the biosensor recognizes the phosphorylated tyrosine. (B) HeLa cells expressing the biosensors indicated above were stimulated with EGF under an epifluorescent microscope, and processed as in Fig. 3A. The number of cells examined in each case was as follows: 11 (Picchu-KTS-X) and 12 (Picchu-mut-KTS-X). (C) HeLa cells expressing the biosensors indicated above were stimulated with EGF under a TPE microscope, and processed as in Fig. 3B. The number of cells examined in each case was as follows: 5 (Picchu-KTS-X) and 7 (Picchu-mut-KTS-X).

950 nm [31]. To overcome this problem, we chose a dark variant of YFP, sREACh, which was originally developed as the FRET acceptor in TPE microscopy [12]. Donor quenching was quantified for the measurement of FRET of biosensors containing sREACh as the acceptor [12]. As previously reported, cross-excitation of sREACh at 840 nm excitation was negligible compared to that of Venus (Fig. 1). We added Keima to the biosensor as an internal fluorescent control (Fig. 2). Keima displays a peak of two-photon action cross sections around 860–900 nm with TPE microscopy [32]. Here, we took advantage of this spectral feature of Keima for its usage as an internal fluorescence control. Although we have not tested them, other fluorescent proteins with long Stokes' shift could be substituted for Keima in our FRET biosensor design [33].

Donor preference: Three fluorescence proteins, EGFP, CFP, and mTFP1, were tested as the donor of sREACh. With an epifluorescent microscope, Pippi-PI(3,4)P_2 containing CFP yielded the largest gain on EGF stimulation, followed by one containing mTFP1. However, with a TPE microscope, Pippi-PI(3,4)P_2 containing mTFP1 yielded the largest gain followed by one containing EGFP (Fig. 3B). The two-photon action spectra indicate that mTFP1 and CFP showed the best action cross section at 867 and 857 nm excitation, respectively, while that of GFP was at 930 nm [32,34]. Therefore, optimization of the excitation wavelength in the TPE microscope for the biosensor with EGFP is required. We suggest two possibilities for the superiority of mTFP1 to CFP in TPE microscopy. First, it has been reported that CFP suffers from a reduced fluorescence yield when compared with most members of the fluorescent protein family [29]. Since in the TPE microscope, the two-photon action cross section, a product of the fluorescence quantum yield and the absolute two-photon absorption cross section, indicates the brightness of the fluorescent proteins, the high quantum yield of mTFP1 (0.85) may render this protein suitable as a replacement for CFP as a FRET donor to either a yellow or orange fluorescent proteins [18,34]. TFP1 contains a tyrosine-derived chromophore, while CFP contains a tryptophan-derived chromophore [28]. This could account for the advantage of mTFP1 in TPE microscopy. Another critical difference may be the exposure time for imaging. In TPE microscopy, the incident beam is scanned over the cell. Thus, the exposure time of each pixel was less than 10 ms at most. In contrast, the exposure time of the wide-field epifluorescence microscope was on the order of 100 ms. This difference affects the photostability of the fluorophore, thereby the FRET efficiency.

The other advantage of the use of mTFP1 over CFP and EGFP is the lack of nucleotide sequence homology with sREACh. Except for mTFP1, which is derived from *Clavularia* coral, all other fluorescent proteins used here are derived from *Aequarea* GFP. The high sequence homology between the donor and the acceptor frequently is known to cause recombination when retroviral vectors are used to deliver the genome into the cells [35]. In fact, we took advantage of this feature to establish MDCK cells stably expressing the Pippi-PI(3,4)P_2-KTS biosensor. Based on the fact that the PH domains from different proteins recognize different PtdInss, a series of experiments developed a novel tool for detecting the localization of these lipids in living and fixed cells by fusing the GFP tag to the PH domain. Using this technique, it had been already reported that PIP_3 is enriched in the lateral membrane of the MDCK cells in the mature cyst, while PI(4,5)P_2 is in the apical membrane [22]. Therefore, it is consistent that PI(3,4)P_2, a derivative of PIP_3, was also enriched in the lateral membrane of the cyst [36]. However, compared to the GFP-fused PH domain method, the FRET-based biosensor detects lipid distribution more sensitively and quantitatively. Images obtained with the GFP-PH-based biosensor are substantially affected by the ratio of the surface area of the plasma membrane to the cytosolic volume (surface-to-volume ratio) [37]. Importantly, we could quantify the FRET efficiency in the cyst expressing the biosensors with the wild-type and mutant PH domains to confirm the relative enrichment of PI(3,4)P_2 (Fig. 4).

Although the TPE microscope, but not the conventional confocal microscope, could obtain a full-depth image of the mature spherical cyst, we noted that the Keima/mTFP ratio was biased along the *z*-axis (data not shown). Since the MDCK cyst is spherical, and FRET efficiency along the *x*–*y* axis was not biased to the *x*- or *y*-axis (Fig. 4), it is suspected that such an artifact was primarily because of the highly scattered emissions of Keima and TFP through a cyst, which are dependent on the fluorescent proteins. Therefore, it is necessary to correct such aberration to obtain the FRET images along the *z*-axis. In addition, it is also required to prepare a negative control probe for each experiment because the dynamic range of Pippi-PI(3,4)P_2-KTS is less than that of the original CFP-YFP probe. This might be caused by the addition of Keima at the N-terminus, which may alter the probe structure to decrease FRET.

In summary, we have established a novel probe for TPE usage based on FRET principles, which enabled the detection of PI(3,4)P_2 distribution at the plasma membrane in a three-dimensional structure. We further applied this strategy to develop biosensors for another phospholipid, PIP_3 (Fig. 5), and tyrosine kinase activity (Fig. 6). Applications for other signaling molecules and *in vivo* imaging using newly developed biosensors will help

elucidate the roles of signaling molecules in a wide variety of biological and pathological phenomena.

Acknowledgments

We are grateful to Ms. A. Abe, Y. Inaoka, K. Hirano, Y. Kasakawa, and N. Nonaka for their technical assistance. We also are grateful to Dr. J. Hejna Alan and the staff at the Matsuda Laboratory for their technical advice and helpful input. This work was supported by grants from the Ministry of Education, Culture, Sports, Science, and Technology of Japan. S. Yagi was supported by research fellowships from the Japan Society for the Promotion of Science for Young Scientists.

Appendix A. Supplementary data

Supplementary data associated with this article can be found, in the online version, at doi:10.1016/j.ab.2011.02.021.

References

[1] E. Kiyokawa, K. Aoki, T. Nakamura, M. Matsuda, Spatiotemporal regulation of small GTPases as revealed by probes based on the principle of Förster resonance energy transfer (FRET): implications for signaling and pharmacology, Annu. Rev. Pharmacol. Toxicol. 51 (2010) 337–358.
[2] E.A. Jares-Erijman, T.M. Jovin, Imaging molecular interactions in living cells by FRET microscopy, Curr. Opin. Chem. Biol. 10 (2006) 409–416.
[3] T. Nagai, S. Yamada, T. Tominaga, M. Ichikawa, A. Miyawaki, Expanded dynamic range of fluorescent indicators for Ca^{2+} by circularly permuted yellow fluorescent proteins, Proc. Natl. Acad. Sci. USA 101 (2004) 10554–10559.
[4] M. Ouyang, J. Sun, S. Chien, Y. Wang, Determination of hierarchical relationship of Src and Rac at subcellular locations with FRET biosensors, Proc. Natl. Acad. Sci. USA 105 (2008) 14353–14358.
[5] H.W. Ai, K.L. Hazelwood, M.W. Davidson, R.E. Campbell, Fluorescent protein FRET pairs for ratiometric imaging of dual biosensors, Nat. Methods 5 (2008) 401–403.
[6] K. Aoki, M. Matsuda, Visualization of small GTPase activity with fluorescence resonance energy transfer-based biosensors, Nat. Protoc. 4 (2009) 1623–1631.
[7] T. Okada, M.J. Miller, I. Parker, M.F. Krummel, M. Neighbors, S.B. Hartley, A. O'Garra, M.D. Cahalan, J.G. Cyster, Antigen-engaged B cells undergo chemotaxis toward the T zone and form motile conjugates with helper T cells, PLoS Biol. 3 (2005) e150.
[8] C.D. Allen, T. Okada, H.L. Tang, J.G. Cyster, Imaging of germinal center selection events during affinity maturation, Science 315 (2007) 528–531.
[9] I. Majoul, M. Straub, R. Duden, S.W. Hell, H.D. Soling, Fluorescence resonance energy transfer analysis of protein–protein interactions in single living cells by multifocal multiphoton microscopy, J. Biotechnol. 82 (2002) 267–277.
[10] W.R. Zipfel, R.M. Williams, W.W. Webb, Nonlinear magic: multiphoton microscopy in the biosciences, Nat. Biotechnol. 21 (2003) 1369–1377.
[11] R. Yasuda, Imaging spatiotemporal dynamics of neuronal signaling using fluorescence resonance energy transfer and fluorescence lifetime imaging microscopy, Curr. Opin. Neurobiol. 16 (2009) 551–561.
[12] S. Ganesan, S.M. Ameer-Beg, T.T. Ng, B. Vojnovic, F.S. Wouters, A dark yellow fluorescent protein (YFP)-based resonance energy-accepting chromoprotein (REACh) for Forster resonance energy transfer with GFP, Proc. Natl. Acad. Sci. USA 103 (2006) 4089–4094.
[13] T. Kogure, S. Karasawa, T. Araki, K. Saito, M. Kinjo, A. Miyawaki, A fluorescent variant of a protein from the stony coral Montipora facilitates dual-color single-laser fluorescence cross-correlation spectroscopy, Nat. Biotechnol. 24 (2006) 577–581.
[14] A.L. Szymczak, C.J. Workman, Y. Wang, K.M. Vignali, S. Dilioglou, E.F. Vanin, D.A. Vignali, Correction of multi-gene deficiency in vivo using a single 'self-cleaving' 2A peptide-based retroviral vector, Nat. Biotechnol. 22 (2004) 589–594.
[15] N. Mochizuki, S. Yamashita, K. Kurokawa, Y. Ohba, T. Nagai, A. Miyawaki, M. Matsuda, Spatio-temporal images of growth-factor-induced activation of Ras and Rap1, Nature 411 (2001) 1065–1068.
[16] M. Sato, Y. Ueda, T. Takagi, Y. Umezawa, Production of PtdInsP3 at endomembranes is triggered by receptor endocytosis, Nat. Cell Biol. 5 (2003) 1016–1022.
[17] H. Murakoshi, S.J. Lee, R. Yasuda, Highly sensitive and quantitative FRET-FLIM imaging in single dendritic spines using improved non-radiative YFP, Brain Cell Biol. 36 (2008) 31–42.
[18] H. Ai, J.N. Henderson, S.J. Remington, R.E. Campbell, Directed evolution of a monomeric, bright and photostable version of *Clavularia* cyan fluorescent protein: structural characterization and applications in fluorescence imaging, Biochem. J. 400 (2006) 531–540.
[19] T. Akagi, T. Shishido, K. Murata, H. Hanafusa, v-Crk activates the phosphoinositide 3-kinase/AKT pathway in transformation, Proc. Natl. Acad. Sci. USA 97 (2000) 7290–7295.
[20] K. Kurokawa, N. Mochizuki, Y. Ohba, H. Mizuno, A. Miyawaki, M. Matsuda, A pair of fluorescent resonance energy transfer-based probes for tyrosine phosphorylation of the CrkII adaptor protein in vivo, J. Biol. Chem. 276 (2001) 31305–31310.
[21] H. Yoshizaki, Y. Ohba, K. Kurokawa, R.E. Itoh, T. Nakamura, N. Mochizuki, K. Nagashima, M. Matsuda, Activity of Rho-family GTPases during cell division as visualized with FRET-based probes, J. Cell Biol. 162 (2003) 223–232.
[22] F. Martin-Belmonte, A. Gassama, A. Datta, W. Yu, U. Rescher, V. Gerke, K. Mostov, PTEN-mediated apical segregation of phosphoinositides controls epithelial morphogenesis through Cdc42, Cell 128 (2007) 383–397.
[23] A.L. Pollack, R.B. Runyan, K.E. Mostov, Morphogenetic mechanisms of epithelial tubulogenesis: MDCK cell polarity is transiently rearranged without loss of cell–cell contact during scatter factor/hepatocyte growth factor-induced tubulogenesis, Dev. Biol. 204 (1998) 64–79.
[24] T. Nagai, K. Ibata, E.S. Park, M. Kubota, K. Mikoshiba, A. Miyawaki, A variant of yellow fluorescent protein with fast and efficient maturation for cell-biological applications, Nat. Biotechnol. 20 (2002) 87–90.
[25] K. Aoki, T. Nakamura, K. Fujikawa, M. Matsuda, Local phosphatidylinositol 3,4,5-trisphosphate accumulation recruits Vav2 and Vav3 to activate Rac1/Cdc42 and initiate neurite outgrowth in nerve growth factor-stimulated PC12 cells, Mol. Biol. Cell 16 (2005) 2207–2217.
[26] T. Nishioka, K. Aoki, K. Hikake, H. Yoshizaki, E. Kiyokawa, M. Matsuda, Rapid turnover rate of phosphoinositides at the front of migrating MDCK cells, Mol. Biol. Cell 19 (2008) 4213–4223.
[27] K. Aoki, T. Nakamura, T. Inoue, T. Meyer, M. Matsuda, An essential role for the SHIP2-dependent negative feedback loop in neuritogenesis of nerve growth factor-stimulated PC12 cells, J. Cell Biol. 177 (2007) 817–827.
[28] H.W. Ai, S. Olenych, P. Wong, M. Davidson, R. Campbell, Hue-shifted monomeric variants of Clavularia cyan fluorescent protein: identification of the molecular determinants of color and applications in fluorescence imaging, BMC Biol. 6 (2008) 13.
[29] N.C. Shaner, P.A. Steinbach, R.Y. Tsien, A guide to choosing fluorescent proteins, Nat. Methods 2 (2005) 905–909.
[30] L.E. O'Brien, T.S. Jou, A.L. Pollack, Q. Zhang, S.H. Hansen, P. Yurchenco, K.E. Mostov, Rac1 orientates epithelial apical polarity through effects on basolateral laminin assembly, Nat. Cell Biol. 3 (2001) 831–838.
[31] P.S. Tsai, B. Friedman, A.I. Ifarraguerri, B.D. Thompson, V. Lev-Ram, C.B. Schaffer, Q. Xiong, R.Y. Tsien, J.A. Squier, D. Kleinfeld, All-optical histology using ultrashort laser pulses, Neuron 39 (2003) 27–41.
[32] H. Kawano, T. Kogure, Y. Abe, H. Mizuno, A. Miyawaki, Two-photon dual-color imaging using fluorescent proteins, Nat. Methods 5 (2008) 373–374.
[33] K.D. Piatkevich, J. Hulit, O.M. Subach, B. Wu, A. Abdulla, J.E. Segall, V.V. Verkhusha, Monomeric red fluorescent proteins with a large Stokes shift, Proc. Natl. Acad. Sci. USA 107 (2010) 5369–5374.
[34] S.E. Tillo, T.E. Hughes, N.S. Makarov, A. Rebane, M. Drobizhev, A new approach to dual-color two-photon microscopy with fluorescent proteins, BMC Biotechnol. 10 (2010) 6.
[35] S. Yoshiki, R. Matsunaga-Udagawa, K. Aoki, Y. Kamioka, E. Kiyokawa, M. Matsuda, Ras and calcium signaling pathways converge at Raf1 via the Shoc2 scaffold protein, Mol. Biol. Cell 21 (2010) 1088–1096.
[36] E. Sahai, J. Wyckoff, U. Philippar, J.E. Segall, F. Gertler, J. Condeelis, Simultaneous imaging of GFP, CFP and collagen in tumors in vivo using multiphoton microscopy, BMC Biotechnol. 5 (2005) 14.
[37] M.L. Craske, M. Fivaz, N.N. Batada, T. Meyer, Spines and neurite branches function as geometric attractors that enhance protein kinase C action, J. Cell Biol. 170 (2005) 1147–1158.